# On a Software Joint Velocity Limitation of a Spherical Parallel Manipulator with Coaxial Input Shafts

Alexandre Lê, Guillaume Rance, Fabrice Rouillier, Arnaud Quadrat, Damien Chablat

# On a Software Joint Velocity Limitation of a Spherical Parallel Manipulator with Coaxial Input Shafts

Alexandre Lê[1,2,3(✉)], Guillaume Rance[1], Fabrice Rouillier[2,3], Arnaud Quadrat[1], and Damien Chablat[4]

[1] Safran Electronics and Defense, Massy, France
{alexandre-thanh.le,guillaume.rance,arnaud.quadrat}@safrangroup.com
[2] Inria Paris, Paris, France
{alexandre.le,fabrice.rouillier}@inria.fr
[3] Sorbonne Université, Université de Paris Cité, Institut de Mathématiques de Jussieu Paris Rive Gauche, Paris, France
[4] Nantes Université, École Centrale Nantes, CNRS, LS2N, UMR 6004, Nantes 44000, France
damien.chablat@cnrs.fr

**Abstract.** This article discusses the implementation of a software joint velocity limitation dedicated to a Spherical Parallel Manipulator (SPM) with coaxial input shafts (CoSPM) using a speed control loop. Such an algorithm takes as input the current joint positions as well as the joint reference velocities computed by the speed controller and limit the latter in order to avoid any known singular configuration. This limitation takes into account the workspace properties of the mechanism and the physical characteristics of its actuators. In particular, one takes advantage of the coaxiality of the input shafts of the CoSPM and the resulting unlimited bearing.

A 3-DOF 3-$\underline{\text{R}}$RR Spherical Parallel Manipulator (SPM) [1,2] with coaxial input shafts (CoSPM) [3] has been used in [4] as a device for the inertial Line-Of-Sight (LOS) stabilization. In particular, such a robot was controlled by its joint and operational velocities taking into account its kinematic model. In this respect, a certified singularity-free delimitation of the joint- and workspace has been established to avoid undesired dangerous behavior of the mechanism. However, a speed control strategy does not guaranty that the robot remains in the safe regions especially if the operational speed reference is non-zero. To solve this issue, we propose in this article an algorithmic solution that acts as a software joint velocity limitation. This algorithm requires the knowledge of the Kinematics of CoSPMs that will be recalled in the following section. The reader may refer to [4] for the details on the modeling.

## 1 Preliminary Kinematic Analysis of CoSPMs

Let $\boldsymbol{\theta} \triangleq \left[\, \theta_1 \; \theta_2 \; \theta_3 \,\right]^{\mathsf{T}}$ and $\boldsymbol{\chi} \triangleq \left[\, \chi_1 \; \chi_2 \; \chi_3 \,\right]^{\mathsf{T}}$ denote the active joint and operational vector coordinates of the robot of interest. More precisely, $\chi_1$, $\chi_2$ and $\chi_3$


J. Lenarčič and M. Husty (Eds.): ARK 2024, SPAR 31, pp. 43–52, 2024.
https://doi.org/10.1007/978-3-031-64057-5_6

respectively represent the *bank*, the *elevation* and the *bearing* angles of the sight device given the Euler Tait-Bryan ZYX convention used in [4,5]. Figure 1 recalls the design of the SPM of interest with its parameters and Table 1 its values.

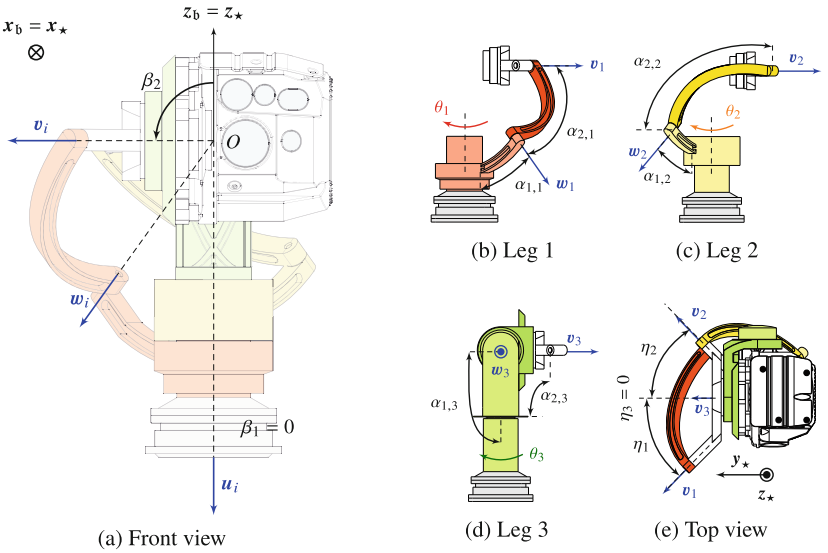


**Fig. 1.** Details on the Coaxial Spherical Parallel Manipulator of interest

**Table 1.** Design parameters of the SPM of interest

| Design parameter | Proximal link | | | Distal link | | | Pivot linkage | | | | |
|---|---|---|---|---|---|---|---|---|---|---|---|
| Notation | $\alpha_{1,1}$ | $\alpha_{1,2}$ | $\alpha_{1,3}$ | $\alpha_{2,1}$ | $\alpha_{2,2}$ | $\alpha_{2,3}$ | $\eta_1$ | $\eta_2$ | $\eta_3$ | $\beta_1$ | $\beta_2$ |
| Value (rad) | $\pi/4$ | $\pi/4$ | $\pi/2$ | $\pi/2$ | $\pi/2$ | $\pi/2$ | $\pi/4$ | $-\pi/4$ | 0 | 0 | $\pi/2$ |

Let $\mathcal{V} = \{(\boldsymbol{\theta}, \boldsymbol{\chi}) \in \mathbb{R}^6 \mid \boldsymbol{f}(\boldsymbol{\theta}, \boldsymbol{\chi}) = \mathbf{0}_{3\times 1}\}$ the algebraic variety describing all the possible solutions to the general geometric model, $\Pi_{\boldsymbol{\theta}}$ (resp. $\Pi_{\boldsymbol{\chi}}$) the projection onto the joint space (*resp.* workspace). Given $\boldsymbol{\theta}_0 \in \Pi_{\boldsymbol{\theta}}(\mathcal{V})$ (*resp.* $\boldsymbol{\chi}_0 \in \Pi_{\boldsymbol{\chi}}(\mathcal{V})$) there exists possibly several solutions to the Forward Kinematic Problem (FKP) $\boldsymbol{f}(\boldsymbol{\theta}_0, \boldsymbol{\chi}) = \mathbf{0}$ (*resp.* Inverse Kinematic Problem (IKP) $\boldsymbol{f}(\boldsymbol{\theta}, \boldsymbol{\chi}_0) = \mathbf{0}$). We then set an initial configuration $(\boldsymbol{\theta}_{\text{init}}, \boldsymbol{\chi}_{\text{init}}) \in \mathcal{V}^\star \subset \mathcal{V}$ and suppose that $\mathcal{V}^\star$ is a simply connected set that does not contain any singularity of $\mathcal{V}$ nor any critical point of $\Pi_{\boldsymbol{\theta}}$ and $\Pi_{\boldsymbol{\chi}}$. Then, for any $\boldsymbol{\theta}_0 \in \Pi_{\boldsymbol{\theta}}(\mathcal{V}^\star)$ (*resp.* $\boldsymbol{\chi}_0 \in \Pi_{\boldsymbol{\chi}}(\mathcal{V}^\star)$) we define $\boldsymbol{\chi}_0$ (*resp.* $\boldsymbol{\theta}_0$) such that $(\boldsymbol{\chi}_0, \boldsymbol{\theta}_0) \in \mathcal{V}^\star$ as being "the" solution of the FKP: $\boldsymbol{\chi}_0 = \text{FKP}(\boldsymbol{\theta}_0)$ (*resp.* IKP: $\boldsymbol{\theta}_0 = \text{IKP}(\boldsymbol{\chi}_0)$) accordingly to the implicit function theorem. In our case, the resulting geometric model of this mechanism is given by

the non-linear system $\boldsymbol{f}(\boldsymbol{\theta}, \boldsymbol{\chi}) = \mathbf{0}_{3\times 1}$ where $f_i(\theta_i, \boldsymbol{\chi}) \triangleq \boldsymbol{w}_i^{\mathsf{T}}(\theta_i)\,\boldsymbol{v}_i(\boldsymbol{\chi}) - \cos(\alpha_{2,i})$, $i \in [\![1,3]\!]$. One can show that all CoSPMs satisfy $\boldsymbol{f}(\theta_1+\epsilon, \theta_2+\epsilon, \theta_3+\epsilon, \boldsymbol{\chi}) = \boldsymbol{f}(\boldsymbol{\theta}, \chi_1, \chi_2, \chi_3+\epsilon)$. A proof is given in [4, Proposition 1].

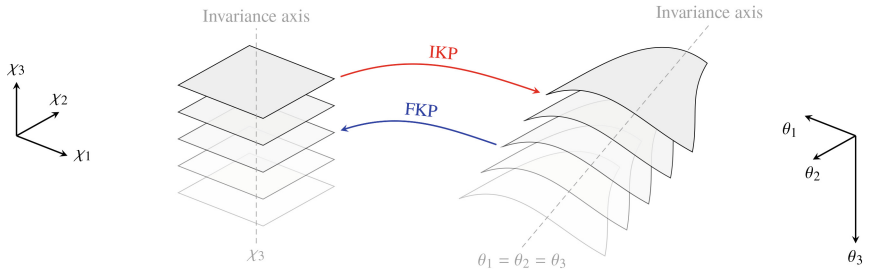


**Fig. 2.** Operational and joint spaces of CoSPMs

As a result, an $\epsilon$-displacement in bearing $\chi_3$ make all the actuators $\theta_i$, $i \in [\![1,3]\!]$ move by $-\epsilon$ without modifying the geometry of the robot. In other words, the singularity loci of all CoSPMs do not vary w.r.t. the bearing axis (thereafter called as *invariance axis*). While the latter is collinear w.r.t. $\chi_3$ in the operational space, the same axis has equation $\theta_1 = \theta_2 = \theta_3$ in the joint space (see Fig. 2). Such a kinematic property allows us to study the workspace $\boldsymbol{\Pi}_{\boldsymbol{\chi}}$ in the $(\chi_1, \chi_2)$-plane.

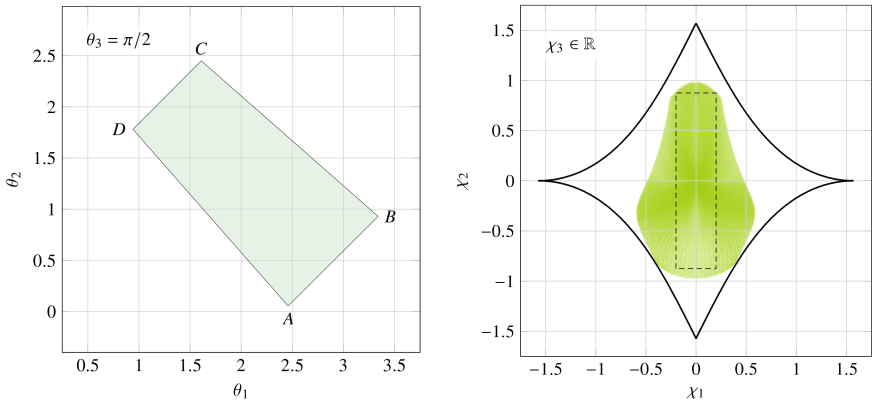


(a) Regular joint space $\mathcal{Q}^\star$ in the $(\theta_1, \theta_2)$-plane at $\theta_3 = \pi/2$

(b) Regular workspace $\mathcal{W}^\star$ (dashed), Type-1 singularity loci (solid) and FKP($\mathcal{Q}^\star$) (green)

**Fig. 3.** Joint- and workspace of the CoSPM of interest

One focuses on a subset $\mathcal{W}^\star \subset \boldsymbol{\Pi}_{\boldsymbol{\chi}}$ called *regular workspace* [6] (see Fig. 3b in dashed) allowing the robot to make ±10° in bank, 100° in elevation with unlimited bearing. Starting from the home initial configuration $\boldsymbol{\chi}_{\text{init}} = \mathbf{0} \leftrightarrow$

$\boldsymbol{\theta}_{\text{init}} = \frac{\pi}{2}\mathbf{1}_{3\times 1}$, one ensures that this leaf of solution does not meet any Type-1 (see Fig. 3b in solid) or Type-2 singularities. Establishing the joint stops requires determining a subset $\mathcal{Q}^\star \subset \Pi_{\boldsymbol{\theta}}$, called *regular joint space*, that is non-singular while allowing the robot to reach any $\boldsymbol{\chi} \in \mathcal{W}^\star$. It is clear that the image of $\mathcal{W}^\star$ at constant bearing $\chi_3 = B$ through the Inverse Kinematics, *i.e.* $\text{IKP}(\mathcal{W}^\star(B))$ is no longer a rectangle lying on a plane but rather a distorted surface in $\mathbb{R}^3$. Given $\mathcal{W}^\star$, the idea is to approximate such a surface by another quadrilateral in the $(\theta_1, \theta_2)$-plane and set $\theta_3$ at an arbitrary value, *e.g.* $\pi/2$ (as shown in Fig. 3a) that is $\mathcal{Q}^\star$. Physically speaking, this means that we immobilize the 3rd leg and check if the robot still reaches all the desired ranges for $\chi_1$ and $\chi_2$ while being indifferent to the value of $\chi_3$. A Kantorovich unicity operator [7,8] applied to $\mathcal{Q}^\star$ guarantees its singularity-freeness and a certified Newton scheme over $\mathcal{Q}^\star$ ensures that $\text{FKP}(\mathcal{Q}^\star)$ (strictly) includes $\mathcal{W}^\star$ as shown in Fig. 3b in green. The latter set is then also *dextrous*. Such information is crucial for the establishment of any strategy limiting the velocities in order to avoid the singular regions.

## 2 Limitation of the Joint Velocities

Let $\dot{\boldsymbol{\theta}} \triangleq \begin{bmatrix} \dot{\theta}_1 & \dot{\theta}_2 & \dot{\theta}_3 \end{bmatrix}^\mathsf{T}$ denote the joint velocity vector and $\dot{\boldsymbol{\chi}} \triangleq \begin{bmatrix} \dot{\chi}_1 & \dot{\chi}_2 & \dot{\chi}_3 \end{bmatrix}^\mathsf{T}$ the vector of the ZYX Tait-Bryan angular rates[1]. As the singularities of the mechanism are independent w.r.t. the $\chi_3$-coordinate, the key idea is to limit $\dot{\boldsymbol{\theta}}$ such that:

**(i)** the characteristics of the actuators (maximum joint velocity $\dot{\theta}_{i,\max}$ and acceleration $\ddot{\theta}_{i,\max}$) are taken into account;
**(ii)** only $\dot{\chi}_1$ (bank rate) and $\dot{\chi}_2$ (elevation rate) are limited in function of the distance between the current pose and its nearest singularity configuration.

It is also worth mentioning that the three coaxial actuators are identical and therefore share the same characteristics ($\dot{\theta}_{i,\max} = \dot{\theta}_{\max}$, $\ddot{\theta}_{i,\max} = \ddot{\theta}_{\max}$, $\forall i \in [\![1,3]\!]$).

**Maximal Joint Velocity and Acceleration.** Regarding **(i)** and the speed control of [4], the joint velocity reference vector (output of the Jacobian matrix) $\dot{\boldsymbol{\theta}}_{\text{c}}$ has to undergo a preliminary saturation $\dot{\boldsymbol{\theta}}$ ensuring that $-\dot{\theta}_{\max} \leq \text{sat}\left(\dot{\theta}_{\text{c},i}\right) = \dot{\theta}_i \leq \dot{\theta}_{\max}$ and $-\ddot{\theta}_{\max} \leq \text{sat}\left(\ddot{\theta}_{\text{c},i}\right) = \ddot{\theta}_i \leq \ddot{\theta}_{\max}$.

Let $T_e$ be the sampling period of the (speed) control loop. The signal $\ddot{\theta}_{\text{c},i}$ is computed at a time $t = kT_e$ using the current and previous values of $\dot{\theta}_{\text{c},i}$ and the Euler approximation $\ddot{\theta}_{\text{c},i}(t = kT_e) = \ddot{\theta}_{\text{c},i}[k] \simeq \frac{1}{T_e}\left(\dot{\theta}_{\text{c},i}[k] - \dot{\theta}_{\text{c},i}[k-1]\right)$.

[1] which is different from the velocity twist coordinates of the platform. See [4] for details.

**Auxiliary Joint Coordinates.** Regarding **(ii)**, an interesting approach involves the use of auxiliary joint coordinates. For this purpose, one can consider a rotational mapping matrix $\boldsymbol{\theta} \mapsto \boldsymbol{q} = \boldsymbol{Q}\boldsymbol{\theta}$ that brings the axis of joint invariance ($\theta_1 = \theta_2 = \theta_3$) to a single entry of the *auxiliary* vector $\boldsymbol{q}$ (*e.g.* the third one as for the orientation vector $\boldsymbol{\chi}$).

**Proposition 1** *Let $\boldsymbol{R}_x(\cdot)$, $\boldsymbol{R}_y(\cdot)$ and $\boldsymbol{R}_z(\cdot)$ denote the usual elementary rotation matrices. The rotational mapping $\boldsymbol{\theta} \mapsto \boldsymbol{q} = \boldsymbol{Q}\boldsymbol{\theta}$ defined by*

$$\boldsymbol{Q} \triangleq \boldsymbol{R}_y\left(-\arctan\left(\frac{\sqrt{2}}{2}\right)\right)\boldsymbol{R}_x\left(\frac{\pi}{4}\right), \tag{1}$$

*brings the geometric invariance to the third auxiliary entry $q_3$.*

***Proof*** Bringing the axis of joint invariance ($\theta_1 = \theta_2 = \theta_3$) to the third entry of a vector yields finding a rotation matrix $\boldsymbol{Q}$ satisfying $\begin{bmatrix} 0 & 0 & 1 \end{bmatrix}^\mathsf{T} = \frac{\sqrt{3}}{3}\boldsymbol{Q}\begin{bmatrix} 1 & 1 & 1 \end{bmatrix}^\mathsf{T}$. This rotation matrix can be viewed as the product of two elementary rotation matrices $\boldsymbol{R}_x(\alpha_x)$ and $\boldsymbol{R}_y(\alpha_y)$. In the case where $\boldsymbol{Q} \triangleq \boldsymbol{R}_y(\alpha_y)\boldsymbol{R}_x(\alpha_x)$, an identification of $\alpha_y$ and $\alpha_x$ leads to $\alpha_x = \frac{\pi}{4} \Rightarrow \alpha_y = -\arctan\left(\frac{\sqrt{2}}{2}\right)$.

Using the auxiliary joint coordinates allows us to represent the *whole* regular joint space $\mathcal{Q}^\star$ in the $(q_1, q_2)$-plane with the free coordinate $q_3 \in \mathbb{R}$ (see Fig. 4b) instead of the $(\theta_1, \theta_2, \theta_3)$-space (Figs. 2 and 3a). Given the previous studies and the design of our robot, the boundary of $\mathcal{Q}^\star$ is composed of four stops $d_i$ that have equation $d_i(q_1, q_2) = a_i\, q_1 + b_i q_2 + c_i$. In our case, we have $a_1 = 0.624$, $a_2 = -1.72$, $a_3 = -0.528$, $a_4 = 1.72$, $c_1 = 0.353$, $c_2 = 3.05$, $c_3 = 0.346$, $c_4 = 1.54$, $b_1 = b_2 = 1$, and $b_3 = b_4 = -1$. The coefficients $a_i$, $b_i$ and $c_i$ are chosen such that $d_i \geq 0$, $\forall i \in [\![1, 4]\!]$ iff $(q_1, q_2) \in \mathcal{Q}^\star$.

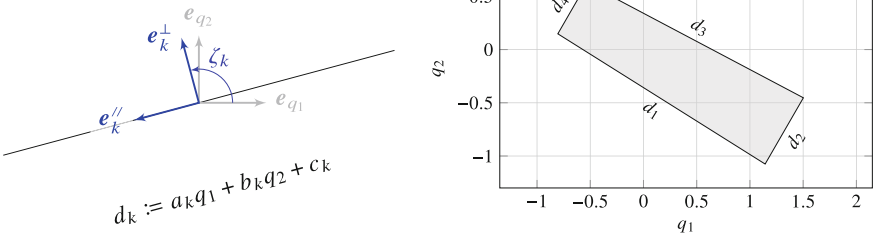


(a) Normal and tangential coordinate transformation

(b) Regular joint space $\mathcal{Q}^\star$ represented in the $(q_1, q_2)$-plane with $q_3$ invariant

**Fig. 4.** Joint space $\mathcal{Q}^\star$ represented in the plane of interest for the joint velocity limitation

The *relative* distance $\delta_i$ between a configuration $\boldsymbol{q}^\star \triangleq \begin{bmatrix} q_1^\star & q_2^\star & q_3^\star \end{bmatrix}^\mathsf{T}$ and a stop $d_i$ is then given by $\delta_i(q_1^\star, q_2^\star) = \left(a_i^2 + b_i^2\right)^{-1/2}\left(a_i q_1^\star + b_i q_2^\star + c_i\right)$. Let $k$ be the

index of the nearest stop $d_k$. The shortest distance to the joint space boundary is then given by $\delta = \delta_k$. Such a formalism is useful for the limitation of the joint velocities as the latter depends on the distance between the current joint configuration $(q_1^\star, q_2^\star)$ and its nearest stop $d_k$.

**Limitation of the Auxiliary Joint Velocities.** In this article, the limitation of the auxiliary joint velocities $\dot{q}_1$ and $\dot{q}_2$ will be applied through their normal and tangential components w.r.t. the nearest stop $d_k$. Let $\{\boldsymbol{e}_{q_1}, \boldsymbol{e}_{q_2}\}$ (*resp.* $\{\boldsymbol{e}_k^\perp, \boldsymbol{e}_k^{/\!/}\}$) denote the canonical basis of the $(q_1, q_2)$-coordinates (*resp.* $(q_k^\perp, q_k^{/\!/})$-coordinates). Figure 4a illustrates the mapping (2) to apply for each stop of Fig. 4b. As a result, one can show that the angles $\zeta_k$ are given by $\zeta_1 = -\pi/2 - |\arctan(a_1)|$, $\zeta_2 = -\pi/2 + |\arctan(a_2)|$, $\zeta_3 = \pi/2 - |\arctan(a_3)|$ and $\zeta_4 = \pi/2 + |\arctan(a_4)|$ given the planar mapping:

$$\begin{bmatrix} \dot{q}_k^\perp \\ \dot{q}_k^{/\!/} \end{bmatrix} = \boldsymbol{R}_k(\zeta_k) \begin{bmatrix} \dot{q}_1 \\ \dot{q}_2 \end{bmatrix} = \begin{bmatrix} \cos(\zeta_k) & \sin(\zeta_k) \\ -\sin(\zeta_k) & \cos(\zeta_k) \end{bmatrix} \begin{bmatrix} \dot{q}_1 \\ \dot{q}_2 \end{bmatrix} \tag{2}$$

where $\dot{q}_k^\perp$ and $\dot{q}_k^{/\!/}$ respectively denote the normal and tangential velocities w.r.t. $d_k$, such that $\boldsymbol{e}_k^\perp$ is oriented towards $d_k$ and $\{\boldsymbol{e}_k^\perp, \boldsymbol{e}_k^{/\!/}\}$ is direct.

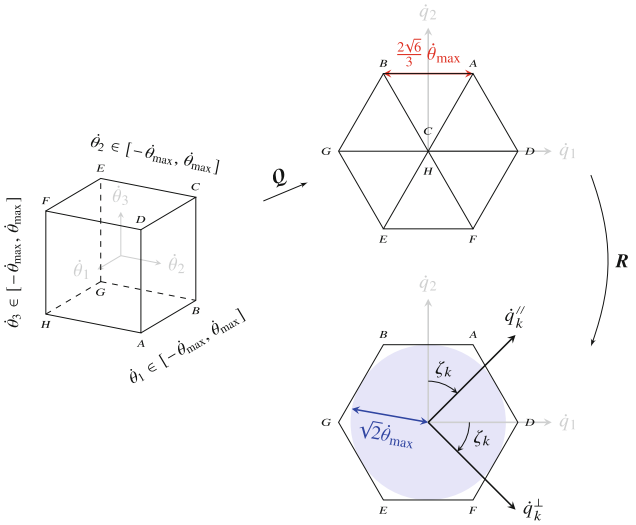


**Fig. 5.** Maximal joint values in the $(\dot{q}_1, \dot{q}_2)$-plane

Limiting the joint velocities given the maximal velocity of the actuators implies that $\dot{\theta}_i \in [-\dot{\theta}_{\max}, \dot{\theta}_{\max}]$. Such a set is a cube in the $(\dot{\theta}_1, \dot{\theta}_2, \dot{\theta}_3)$-space and its projection onto the $(\dot{q}_1, \dot{q}_2)$-plane describes a regular hexagon of side $\frac{2}{3}\sqrt{6}\,\dot{\theta}_{\max}$, as shown in Fig. 5. Such a shape describes the set of all the admissible joint velocities in the $(\dot{q}_1, \dot{q}_2)$-plane. For purpose of simplification, one focuses

on a subset of this regular hexagon that is the inscribed disk of radius $\sqrt{2}\,\dot{\theta}_{\max}$, so that $\dot{q}^{\perp}_{k,\max}$ is defined uniformly in the $(\dot{q}_1, \dot{q}_2)$-plane by

$$\dot{q}^{\perp}_{k,\max} = \sqrt{2}\,\dot{\theta}_{\max}. \tag{3}$$

The same logic applies for the maximal normal acceleration $\ddot{q}^{\perp}_{k,\max} = \sqrt{2}\,\ddot{\theta}_{\max}$.

Once the maximal joint normal velocity is determined in function of $\dot{\theta}_{\max}$, the behavior of the joint velocity between the nominal case and near a joint stop must be defined. Figure 6 plots the joint velocity limitation profile of the normal joint velocity $\dot{q}^{\perp}_{k}$ w.r.t. the distance of the current configuration to the nearest stop $\delta$.

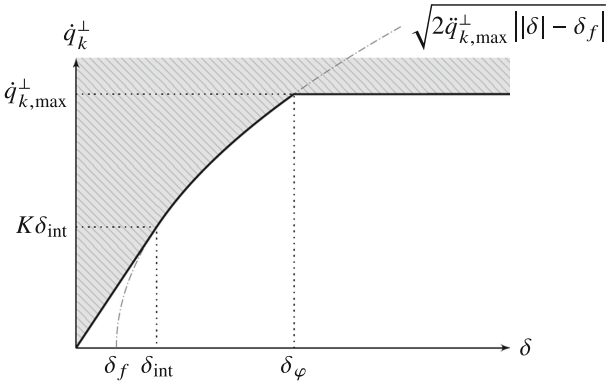


**Fig. 6.** Joint velocity profile w.r.t. the distance to the nearest stop $\delta$

The resulting velocity profile in question can be divided into three distinct zones. Each of them has its own distinctive deceleration law although the continuity of the overall function:

- $[0, \delta_{\text{int}}]$ is the closest zone to the stop $d_k$ in which the limited joint speed is proportional to $\delta$, such that $-K\delta \leq \dot{q}^{\perp}_{k,\text{lim}} \leq K\delta$, where $K$ is a gain. As $\delta$ is small, this allows the joint normal velocity to reach 0 without abusively using the actuators. The parameter $\delta_{\text{int}}$ defines the *linear zone* threshold and is set as $\delta_{\text{int}} = \ddot{q}^{\perp}_{k,\max}/K^2$.
- $[\delta_{\text{int}}, \delta_\varphi]$ is the *maximal deceleration* zone defined by the parameters $\delta_f$ and $\delta_\varphi$ such that $\delta_f = \ddot{q}^{\perp}_{k,\max}/(2K^2) = \delta_{\text{int}}/2$ and $\delta_\varphi = \delta_f + (\dot{q}^{\perp}_{k,\max})^2/(2\ddot{q}^{\perp}_{k,\max})$. In this zone, the joint normal velocity is bounded by $|\dot{q}^{\perp}_{k,\text{lim}}| \leq (2\ddot{q}^{\perp}_{k,\max}||\delta| - \delta_f|)^{1/2}$. Such a condition allows the robot to stop with a zero speed.
- $\delta > \delta_\varphi$ is the *nominal* zone in which the joint position is sufficiently far from the nearest stop $d_k$ (and thus, any singularity). In fact, $\delta_\varphi$ is the joint limitation threshold. Accordingly, the normal velocity component $\dot{q}^{\perp}_{k}$ is only limited by the maximal velocity of the actuators $\dot{\theta}_{\max}$ (or $\dot{q}^{\perp}_{k,\max}$).

Finally, the limited joint velocity $\dot{q}^{\perp}_{k,\mathrm{lim}}$ can be piecewise-defined as:

$$\dot{q}^{\perp}_{k,\mathrm{lim}} = \begin{cases} \min\left(\dot{q}^{\perp}_{k}, \operatorname{sgn}(\delta)\dot{q}^{\perp}_{k,\max}\right) & (\text{if } |\delta| > \delta_{\varphi}) \\ \min\left(\dot{q}^{\perp}_{k}, \operatorname{sgn}(\delta)\sqrt{2\ddot{q}^{\perp}_{k,\max}\left||\delta| - \delta_{f}\right|}\right) & (\text{if } \delta_{\mathrm{int}} < |\delta| \leq \delta_{\varphi}) \\ \min\left(\dot{q}^{\perp}_{k}, K\delta\right) & (\text{if } |\delta| \leq \delta_{\mathrm{int}}) \end{cases} \tag{4}$$

In order to ensure that the robot stops at the boundary of $\boldsymbol{Q}^{\star}$, one can limit the tangential one $\dot{q}^{/\!/}_{k}$ such that

$$q^{/\!/}_{k,\mathrm{lim}} = \begin{cases} \dfrac{q^{/\!/}_{k} q^{\perp}_{k,\mathrm{lim}}}{q^{\perp}_{k}} & (\text{if } q^{\perp}_{k} \neq 0) \\ q^{/\!/}_{k} & (\text{otherwise}) \end{cases} \tag{5}$$

Once the normal $\dot{q}^{\perp}_{k}$ and tangential $\dot{q}^{/\!/}_{k}$ joint velocities are limited, one can go back to $\dot{\boldsymbol{q}}$- and the (original) $\dot{\boldsymbol{\theta}}$-coordinates through the (orthogonal) matrices $\boldsymbol{R}^{\mathsf{T}}_{k}$ and $\boldsymbol{Q}^{\mathsf{T}}$. Finally, Fig. 7 depicts the diagram of the joint velocity limitation.

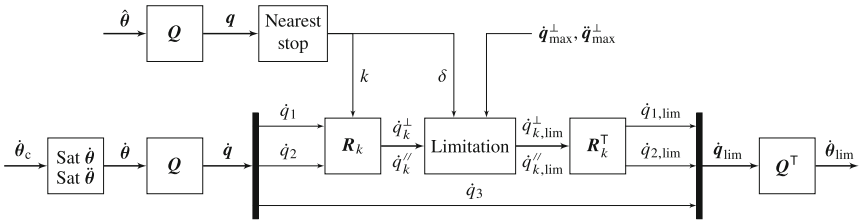


**Fig. 7.** Transformations involved in the limitation of the joint velocities

## 3 Example of Simulation

In this section, we implement the joint velocity limitation algorithm of Fig. 7 using MATLAB 2022a & Simulink. We set $K = 100$, $\dot{\theta}_{\max} = 2\,\mathrm{rad/s}$ and $\ddot{\theta}_{\max} = 20\,\mathrm{rad/s^2}$ which implies that $\delta_f = 0.0014\,\mathrm{rad}$, $\delta_{\mathrm{int}} = 0.0028\,\mathrm{rad}$, $\delta_{\varphi} = 0.1428\,\mathrm{rad}$, with $\dot{q}_{\max} = 2.8284\,\mathrm{rad/s}$ and $\ddot{q}_{\max} = 28.28\,\mathrm{rad/s^2}$. Starting from the home configuration, we consider the following threefold scenario:

$$\dot{\theta}_{c,1} = \begin{cases} 0 & (t \leq 0) \\ -0.5 & (0 < t \leq 2.5) \\ 0.5 & (t > 2.5) \end{cases}, \qquad \dot{\theta}_{c,2} = -\dot{\theta}_{c,1}, \qquad \dot{\theta}_{c,3} = \begin{cases} 0 & (t \leq 3) \\ 0.5 & (t > 3) \end{cases}$$

The current joint vector $\hat{\boldsymbol{\theta}}$ is being estimated by integration of $\dot{\boldsymbol{\theta}}_{\mathrm{lim}}$ (the actuator loop is assumed ideal). Moreover, one can deduce the output angular rates $\dot{\boldsymbol{\chi}}_{\mathrm{lim}}$

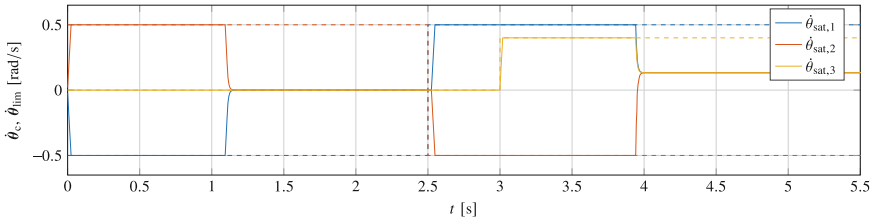


(a) $\dot{\boldsymbol{\theta}}_{\mathrm{c}}$ (dashed) and $\dot{\boldsymbol{\theta}}_{\mathrm{lim}}$ (solid)

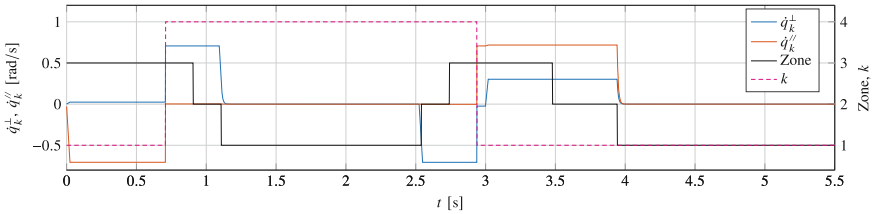


(b) Normal and tangential joint velocities w.r.t. $k^{\mathrm{th}}$ stop and zone flag (3: nominal, 2: maximal deceleration, 1: linear)

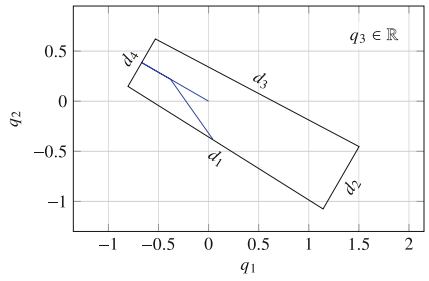


(c) Trajectory in the $(q_1, q_2)$-plane

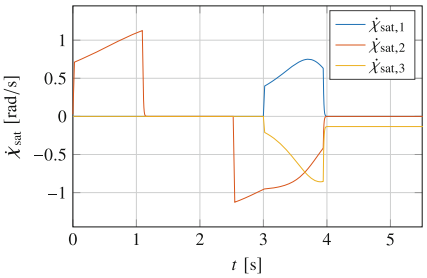


(d) Angular rates $\dot{\boldsymbol{\chi}}_{\mathrm{lim}} \triangleq \boldsymbol{J}\dot{\boldsymbol{\theta}}_{\mathrm{lim}}$

**Fig. 8.** Results of Scenario 1

given that $\dot{\boldsymbol{\chi}}_{\mathrm{lim}} \triangleq \boldsymbol{J}\dot{\boldsymbol{\theta}}_{\mathrm{lim}}$. Results of this simulation is shown in Fig. 8: Fig. 8a displays the actual joint values whereas Fig. 8b shows the limited auxiliary coordinates.

First, the physical constraints of the actuators are taking into account as seen in Fig. 8a. Indeed, the joint velocity references $\dot{\theta}_{\mathrm{c},1}$ and $\dot{\theta}_{\mathrm{c},2}$ instantly change from 0 to $\pm 0.5\,\mathrm{rad/s}$. Despite the discontinuity of these reference signals, the corresponding limited joint velocities $\dot{\theta}_{\mathrm{lim},i}$ are continuous, starting with a slope of 20 (in absolute value) which is in fact the maximal acceleration $\ddot{\theta}_{\max}$ (in $\mathrm{rad/s^2}$). The same thing happens for $\dot{\theta}_{\mathrm{sat},3}$ at $t = 3\,\mathrm{s}$. Requirement **(i)** is here respected. Moreover, setting $\dot{\theta}_1 = -\dot{\theta}_2$ enables a motion in elevation $\chi_2$ (its rate is non-zero as shown in Fig. 8d). The latter makes the robot leave the safe joint region $\boldsymbol{Q}^{\star}$ by going towards $d_4$ (see Fig. 8b and 8c). However, the joint velocity limitation allows the robot to decelerate from $t = 1.09\,\mathrm{s}$ until it stops at $t = 1.15\,\mathrm{s}$. More precisely, according to Fig. 8b, the mechanism enters the

maximal deceleration zone of the $4^{\text{th}}$ stop at $t = 0.9\,\text{s}$ without immediately reducing the normal joint velocity $\dot{q}_4^{\perp}$ as it is already lower than the maximal velocity allowed in this zone. The linear zone of $d_4$ is reached at $t = 1.1\,\text{s}$ and all the legs stop moving until the opposite motion is made at $t = 2.5\,\text{s}$. This allows the robot to turn back until the $3^{\text{rd}}$ leg is actuated at $t = 3\,\text{s}$. As a result, the trajectory of the robot bifurcates (see Fig. 8c and 8d) by making a motion in bank and bearing so that the $1^{\text{st}}$ stop is reached without being crossed at $t = 3.95\,\text{s}$. Furthermore, one can see in Fig. 8d that the vanishing rates at the end are $\dot{\chi}_1$ (bank) and $\dot{\chi}_2$ (elevation). Only $\dot{\chi}_3$ is non-zero being at $-0.13\,\text{rad/s}$. Requirement **(ii)** is here respected.

## 4 Conclusions and Outlook

This paper explored a joint velocity limitation strategy applied to a CoSPM. In particular, it has been shown that such an algorithm took into consideration the workspace properties as well as the physical features of the actuators (maximal velocity and acceleration). Part of further studies will study critical cases (*e.g.* bisectors, vertices) and explore other limitation strategies in order to compare them with the one in this paper. Finally, future works will better take into account the shape of the admissible joint velocity space.

## References

1. Gosselin, C.M., Sefrioui, J., Richard, M.J.: On the direct kinematics of spherical three-degree-of-freedom parallel manipulators of general architecture. J. Mech. Des. **116**(2), 594–598 (1994). https://doi.org/10.1115/1.2919419
2. Shintemirov, A., Niyetkaliyev, A., Rubagotti, M.: Numerical optimal control of a spherical parallel manipulator based on unique kinematic solutions. IEEE/ASME Trans. Mechatron. **21**, 1–1 (2015)
3. Tursynbek, I., Shintemirov, A.: Infinite torsional motion generation of a spherical parallel manipulator with coaxial input axes. In: 2020 IEEE/ASME International Conference on Advanced Intelligent Mechatronics (AIM), pp. 1780–1785 (2020)
4. Lê, A., Rouillier, F., Rance, G., Chablat, D.: Inertial line-of-sight stabilization using a 3-DOF spherical parallel manipulator with coaxial input shafts. In: 11th International Symposium on Optronics in Defense & Security. Bordeaux, France (2024). https://inria.hal.science/hal-04483255
5. Lê, A., Chablat, D., Rance, G., Rouillier, F.: On the certification of the kinematics of 3-DOF spherical parallel manipulators. Maple Trans. **3**, 1–17 (2023). https://doi.org/10.5206/mt.v3i2.15660
6. Chablat, D., Wenger, P., Merlet, J.-P.: An interval analysis based study for the design and the comparison of three-degrees-of-freedom parallel kinematic machines. Int. J. Robot. Res. **23**(6), 615–624 (2004)
7. Kantorovich, L.V.: On Newton's method for functional equations. Funct. Anal. Appl. Math. **59**(7), 1237–1240 (1948)
8. Demidovitch, B., Maron, I.: Éléments de calcul numérique. MIR - Moscou (1973)